Optical security verification by synthesizing thin films with unique polarimetric signatures

ARTUR CARNICER[1,*], ORIOL ARTEAGA[1,2], ESTHER PASCUAL[1,2], ADOLF CANILLAS[1,2], SANTIAGO VALLMITJANA[1], BAHRAM JAVIDI[3], AND ENRIC BERTRAN[1,2]

[1]Universitat de Barcelona (UB), Facultat de Física, Departament de Física Aplicada i Òptica, Martí i Franquès 1, 08028 Barcelona, Catalunya (Spain)
[2]FEMAN Group, Institut de Nanociència i Nanotecnologia de la Universitat de Barcelona (IN2UB), 08028 Barcelona, Catalunya (Spain)
[3]Electrical and Computer Engineering Department, University of Connecticut, 371 Fairfield Road, Storrs, Connecticut 06269 (USA)
[*]Corresponding author: artur.carnicer@ub.edu

Compiled October 18, 2015

This letter reports the production and optical polarimetric verification of codes based on thin-film technology for security applications. Because thin-film structures display distinctive polarization signatures, this data is used to authenticate the message encoded. Samples are analyzed using an imaging ellipsometer able to measure the 16 components of the Mueller matrix. As a result, the behavior of the thin-film under polarized light becomes completely characterized. This information is utilized to distinguish among true and false codes by means of correlation. Without the imaging optics the components of the Mueller matrix become noise-like distributions and, consequently, the message encoded is no longer available. Then, a set of Stokes vectors are generated numerically for any polarization state of the illuminating beam and thus, machine learning techniques can be used to perform classification. We show that successful authentication is possible using the k-nearest neighbors algorithm in thin-films codes that have been anisotropically phase-encoded with pseudo-random phase code.

OCIS codes: *(100.4998) Pattern recognition, optical security and encryption, (260.5430) Polarization, (240.0310) Thin films, (240.2130) Ellipsometry and polarimetry, (150.0150) Machine vision.*

http://dx.doi.org/10.1364/OL.XX.XXXXXX

Nowadays, authentication of the information encoded in a physical support such as barcodes or quick response QR codes raises a real concern among potential users. The encoded information can be harmful since its origin cannot be validated easily. For instance, malicious codes can direct the browser to a harmful site without the user knowledge. Or tampered hardware with apparently legitimate codes may compromise an entire critical system. Recently, different methods have been proposed to help authenticate QR codes i.e. printing the code with special inks made with nanoparticles [1], use of random phase-only tags as an extra security layer [2] or to produce codes with metal nanoparticles [3]. In these cases, some physical properties of the code have to be measured in order to verify the origin of the message. In particular, the analysis of the state of polarization of the light that interacts with the code provides critical information that enables to classify the sample as trusted or non-trusted [3].

Thin film technology offers a huge number of possibilities for generating multilayer structures. Thus, the combination of different deposition technologies and treatments (physical and chemical vapor deposition, PVD and CVD respectively, thermal annealing, plasma surface treatments, etc), materials and compositions, number of layers and shuffling, layer thicknesses and combinations, homogeneous films and anisotropic films, internal structures of the films, surface structures, among others, provide great freedom of choice of parameters for many different and sophisticated optical effects [4]. The thin-film polarimetric encoded QR codes can offer unique characteristics: hidden parameters to the naked eye, immense difficulty to reproduce the QR item without a precise knowledge of all the deposition parameters, additional sensing parameters such as the wavelength and the angle of incidence needed for validation, fast image treatment algorithms to determine the authenticity or falsity of the QR logo, even in conditions of lack of information or disposition of a portion of the item. A final option offering this modified QR technology is the fabrication of singular and exclusive QR items, with no possibility of reproduction.

In this paper, we propose to use codes produced with thin-film technology for security applications. Thin-films structures illuminated with polarized light produce characteristic information that is used for recognition and identification purposes. Experimental measures are carried out by using an imaging polarimeter. This device enables the characterization of the components of the Mueller matrix of the thin-film. The use of this polarimetric method means a clear advantage when compared with previous studies since the knowledge of the Mueller matrix provides information about any possible polarization state. Validation of the code is carried out using image correlation or classification algorithms.

The paper is organized as follows: first, we explain how the thin-film samples are generated. Second, we introduce an effective technique that enables measuring the Mueller coefficients of the code. In order to make more difficult the reproduction of the code, anisotropy is induced by placing pseudorandom phase masks such as small strips of scotch tape placed at random directions. Correlation is used to distinguish among true and false codes. Finally, the Mueller matrix is obtained in non-imaging conditions and thus its components become noise-like signals. This fact is used to perform authentication by means of machine learning techniques.

QR samples were fabricated by standard lithographic and deposition technologies on flat glass substrates (microscopy slides of 25 mm × 75 mm). The QR code used is shown in Fig. 1(a); the message encoded is a telephone number (0034934...). For the lithographic process we used AZ5214E photoresist deposited directly on a pre-cleaned glass by spin coating up to 6000 revolutions per minute during 30 s. The resulting thicknesses were typically of 100-200 nm, which provided satisfactory results after UV exposition (200 W Hg Arc lamp) during 47 s through the mask (see Fig. 1(b)). Finally, we carried out the development process using AZ400K developer (30÷120 in water) during around one minute. In order to have reproducible results, various trials were done to find the suitable parameters for the different steps (spin-coating parameters, cure time, exposition time, developer time, etc.) [4, 5].

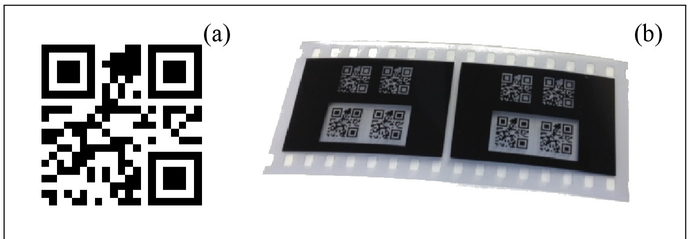

Fig. 1. (a) QR code. The message encoded is 0034934... (b) Negative and positive QR photography, based on a Kodalith-like film, to be used as a lithographic mask.

Samples with two different thin-films on glass were produced: a semi-transparent and absorbent film, Cr (20 nm thick) and a low absorbing film, Ta_2O_5 (120 nm thick). Deposition processes were carried out by radio-frequency (RF) sputtering using targets of pure Cr and pure Ta of 75 mm of diameter, respectively [5]. The deposition parameters are listed in table 1. For the Ta_2O_5 film, a reactive process was performed using a gas mixture of O_2 / Ar of 6÷49 standard cubic centimeters per minute (sccm). The RF power supplied along with the process total pressure and the distance between target and substrate given place to a quite transparent TaO_x in the visible range, very close to the stoichiometry ratio ($x = 2.5$). After the deposition process, both samples were submitted to a lift-off process using a sonic bath of acetone, which removed the lithographic mask and the film deposited on it. A photo of the samples is shown in Fig. 2.

Ellipsometry measurements were made with a home-made imaging Mueller matrix ellipsometer. This instrument uses monochromatic light together with a dual rotating compensator to produce 16 images corresponding to every elements of the Mueller matrix of the sample. The working principle of this imaging ellipsometer is the same we previously described for a Mueller matrix microscope [6]. It is based on the frequency analysis of the intensity captured at every pixel of a CMOS camera while two compensators, continuously rotating at different frequencies, modulate the polarization of light. A teleobjective

Table 1. Deposition parameters of QR samples using RF magnetron sputtering from Cr and Ta targets.

QR sample	Cr / glass	Ta_2O_5 / glass
Developer time (s)	45	45
Thickness (nm)	20	120
Target	Cr	Ta
Target-substrate distance (cm)	8	8
Gas mixture	Ar	Ar / O_2
Flow ratio (sccm)	20	49 / 6
Pressure (Pa)	1.0	1.0
RF power (W)	50	160

Fig. 2. Thin-films produced by RF magnetron sputtering through a QR photolithographic mask having a structure film / QR Mask / glass. Left: Ta_2O_5 / QR / glass (120 nm thick). Right: Cr / QR / glass (20 nm thick).

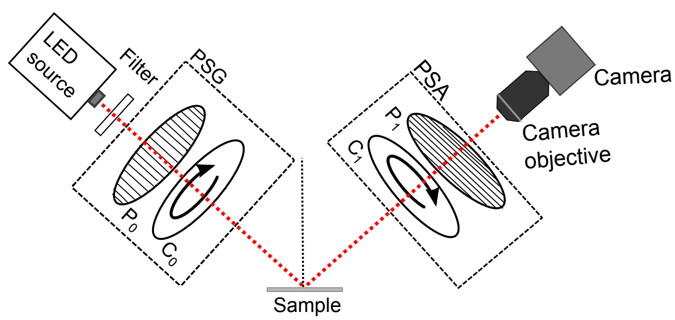

Fig. 3. Diagram of the imaging Mueller matrix ellipsometer. PSG and PSA state, respectively, for polarization state generator and polarization state analyzer. The PSG and the PSA are composed of a polarizer (P) and a rotating compensator (C).

lens was placed in front of the camera to image the QR codes. The angle of incidence in all measurements was 56° and the selected wavelength of analysis was 535 nm. A diagram of the instrument is shown in Fig. 3.

If light interacts with an isotropic sample, 8 out of the 16 components of the Mueller matrix are zero and it is highly symmetric [7]. In this case **M** reads

$$\mathbf{M} = \begin{bmatrix} 1 & -N & 0 & 0 \\ -N & 1 & 0 & 0 \\ 0 & 0 & C & S \\ 0 & 0 & -S & C \end{bmatrix}, \quad \textbf{(1)}$$

where $N = \cos(2\Psi)$, $C = \sin(2\Psi)\cos(\Delta)$ and $N = \sin(2\Psi)\sin(\Delta)$. The ellipsometric angles Ψ and Δ are related to the complex Fresnel reflection coefficients for $p-$ and $s-$ polarized light (r_{pp} and r_{ss} respectively) by means of

$$\rho = \frac{r_{pp}}{r_{ss}} = \tan(\Psi)\exp(i\Delta). \quad \textbf{(2)}$$

Note that ρ is a complex distribution that summarizes the polarimetric information of the measured samples. Figures 4(a) and 4(b) show the 16 Mueller matrix images measured for the Cr and and Ta_2O_5 samples. Note that they follow the symmetry of Eq. (1).

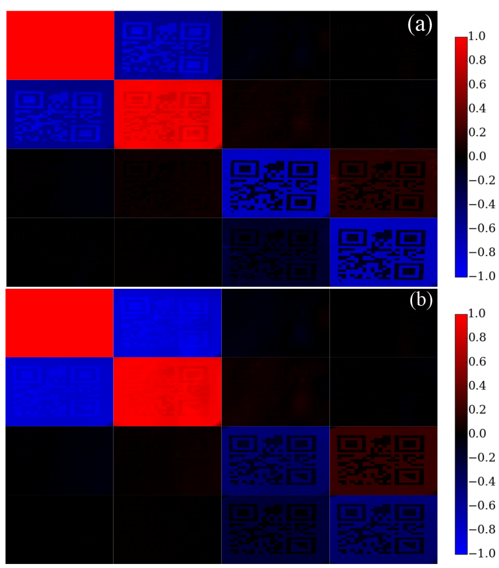

Fig. 4. Mueller images: (a) Cr sample and (b) Ta_2O_5 sample.

From the information contained in the Mueller matrix images we calculate complex distributions ρ_{Cr} and $\rho_{Ta_2O_5}$. We show that ρ can be used for recognition purposes using phase-only correlation [8]. In 2007, Nomura used correlation to perform pattern recognition using holographic based polarimetric information [9]. Figures 5(a) and 5(b) display the autocorrelation for the Cr sample and the cross-correlation between Cr and Ta_2O_5 samples respectively. Results demonstrate that two identical QR codes produced with different homogeneous materials can be distinguished using correlation between parameters derived from a polarimetric analysis.

Because our polarization characterization method determines the complete Mueller matrix [6], the complexity of the QR codes could be enhanced by using layers and/or substrates of materials with optical anisotropy. When dealing with anisotropic samples, the number of polarimetric parameters intrinsic to the reflection process increases from 3 (the real and the imaginary part of the complex reflectance ratio plus the unpolarized reflectivity) to 7 independent parameters if depolarization is not considered [7]. For this reason we generated

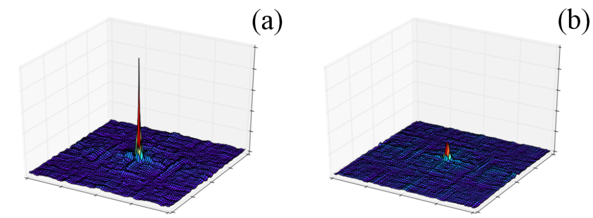

Fig. 5. Phase-only correlations for identification of thin film encoded QR codes with phase masks [see Eq. (2)]. (a) $|\rho_{Cr} \otimes \rho_{Cr}|$. (b) $|\rho_{Cr} \otimes \rho_{Ta_2O_5}|$. Values are normalized to the autocorrelation maximum. Here $\otimes$ denotes phase-only correlation.

new samples by attaching pseudorandom phase masks using randomly oriented strips of scotch tape to the original thin-film structures. The corresponding Mueller matrix images are shown in Figs. 6(a) and 6(b). Interestingly, none of the 16 components of the Mueller-matrix images vanishes.

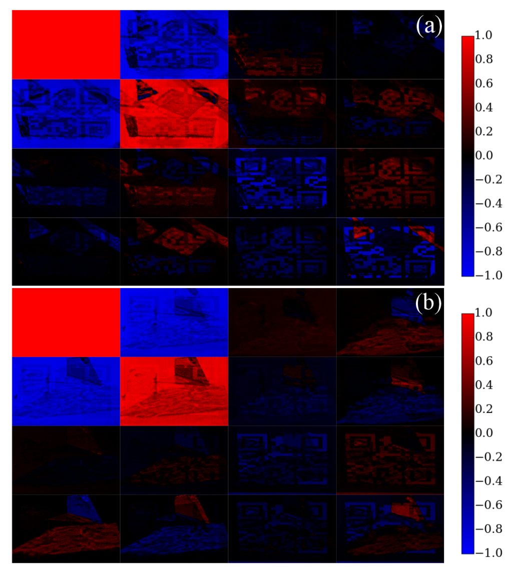

Fig. 6. Mueller images:(a) Cr sample + scotch tape. (b) Ta_2O_5 sample + scotch tape.

In this case the calculation of the Fresnel coefficients becomes more complex because two extra Fresnel coefficients, r_{ps} and r_{sp}, need to be considered. r_{ps} and r_{sp} describe the transformation of pure p-(s-) polarized light to result in some s-(p-) polarized upon reflection. Therefore ellipsometry measurements on anisotropic samples are usually reported using the three complex ratios $\rho = r_{pp}/r_{ss}$, $\rho_{ps} = r_{ps}/r_{ss}$ and $\rho_{sp} = r_{sp}/r_{ss}$. These coefficients for the Mueller matrices of Figs. 6(a) and 6(b) are calculated using the Cloude sum decomposition [7] which, by considering only the largest eigenvector of the decomposition, allows finding the closest Jones matrix corresponding to an experimental Mueller matrix. Then, phase-only correlation is used again to determine whether sample Cr is detected or not. Table 2 shows the normalized phase-only cross-correlation maxima for the Fresnel coefficients. Since the three values are very small, the Ta_2O_5 sample is rejected. For samples with scotch tape, phase-only correlation is again a good method to distinguish among the two classes.

Taking into account that the samples are phase-encoded, the Mueller components images become noise distributions if the

Table 2. Phase-only cross-correlations maxima for the samples with pseudorandom phase masks, that is, scotch tape. Values are normalized to the corresponding autocorrelation maximum.

$\lvert\rho^{\mathrm{Cr}} \otimes \rho^{\mathrm{Ta_2O_5}}\rvert(0,0)$	0.040
$\lvert\rho^{\mathrm{Cr}}_{\mathrm{ps}} \otimes \rho^{\mathrm{Ta_2O_5}}_{\mathrm{ps}}\rvert(0,0)$	0.020
$\lvert\rho^{\mathrm{Cr}}_{\mathrm{sp}} \otimes \rho^{\mathrm{Ta_2O_5}}_{\mathrm{sp}}\rvert(0,0)$	0.014

camera objective is removed [2]. Even in this case, it is possible to distinguish between the two codes using machine learning algorithms. Note that the code can be validated or rejected without accessing the information encoded. Let $\mathbf{S} = (I, Q, U, V)$ be the Stokes vector of a input beam. The polarization state of the beam after interacting with a sample described by the Mueller matrix $\mathbf{M}$ is simply $\mathbf{S}' = \mathbf{MS}$. In order to generate enough information to perform successful classification, we calculate the Stokes vector $\mathbf{S}'$ when the sample is illuminated with linearly polarized light. The polarization angle φ ranges from 0° to 180° with a step size of 0.1°. This is equivalent to multiplying the experimental Mueller matrix images $\mathbf{M}$ by the Stokes vector $\mathbf{S} = (1, \cos(2\varphi), \sin(2\varphi), 0)$. The resulting Stokes vector ensemble $\mathbf{S}' = \mathbf{MS} = (I', Q', U', V')$ is composed of four groups of 1800 images. For classification purposes we take the 256-bin histograms of the 1800 images for each group I', Q', U' and V'. The degree of polarization (DoP) is also calculated. Figure 7 shows some of the histograms of component V' for the two thin-film codes for selected values of φ.

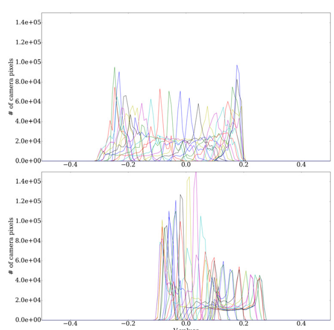

Fig. 7. Histograms for some of the V' images; $\varphi = 0°, 5°, 10°, 15°, 20°, \ldots, 170°$, and 175°. Cr + scotch tape (top) and Ta_2O_5 + scotch tape (bottom).

Among the different machine learning techniques, we selected the k-nearest neighbors (kNN) algorithm [10] because this method is unsupervised, easy to implement but very powerful. kNN tries to determine the class the current sample belongs by considering the majority of the k closest samples of the training set. Calculations are carried out using the scikit-learn library [11]. The optimal number for k is highly dependent of the problem and here the number of neighbors k is set to 1. The data set was divided into training and test sets using a hold-out strategy: the training set was generated by selecting randomly 900 samples of both classes. The figure of merit used for the assessment of the classification is the mean accuracy defined as the total number of correctly classified samples divided by the total number of test samples [12]. The classification algorithm was run 50 times using different training sets. Results are presented in Table 3: In our experiments, error free classification is possible using the information contained in the histograms of components U' or V' or by means of the DoP.

Table 3. Classification mean accuracy, k=1

I'	Q'	U'	V'	DoP
72%	78%	100%	100%	100%

In summary, we demonstrated that codes produced using thin-films technology can be used in security applications. These codes produce a unique polarimetric signature. Characterization is carried out using a polarimeter able to measure the Mueller matrix of the samples. Codes are validated using correlation between polarimetric coefficients. Since the samples can be phase-encoded the polarimeter can also work in non-imaging conditions. In this way the polarimetric signals become noise distributions and the encoded information is no longer accessible. Nevertheless, codes can be still authenticated with the help of machine learning techniques. The proposed polarimetric optical thin film security can be applied to a variety of optical security and encryption approaches [13–17].

Funding. Ministerio de Economía y Competitividad (Spain) projects FIS2013-46475, AGAUR of the Generalitat de Catalunya project 2014SGR0948 and European Union (Marie Curie IIF Fellowship, PIIF-GA-2012-330513). B. Javidi wishes to thank support from Honeywell.

Acknowledgments. The authors are grateful to Arevik Musheghyan-Avetisyan by her assistance in the lithographic process and Dr. Pedro Latorre for helpful discussions on machine learning techniques.

REFERENCES

1. J. M. Meruga, W. M. Cross, P. S. May, Q. Luu, G. A. Crawford, and J. J. Kellar, Nanotechnology **23**, 395201 (2012).
2. A. Markman, B. Javidi, and M. Tehranipoor, IEEE Photon. J. **6**, 1–9 (2014).
3. A. Carnicer, A. Hassanfiroozi, P. Latorre-Carmona, Y.-P. Huang, and B. Javidi, Opt. Lett. **40**, 135–138 (2015).
4. V.-M. Freire, C. Corbella, E. Bertran, S. Portal-Marco, M. Rubio-Roy, and J.-L. Andújar, J. Appl. Phys. **111**, 124323 (2012).
5. C. Corbella, B. Echebarria, L. Ramírez-Piscina, E. Pascual, J. Andújar, and E. Bertran, Appl. Phys. Lett. **87**, 213117 (2005).
6. O. Arteaga, M. Baldrís, J. Antó, A. Canillas, E. Pascual, and E. Bertran, Appl. Opt. **53**, 2236–2245 (2014).
7. O. Arteaga, Thin Solid Films **571**, 584–588 (2014).
8. J. L. Horner and P. D. Gianino, Appl. Opt. **23**, 812–816 (1984).
9. T. Nomura and B. Javidi, Opt. Lett. **32**, 2146–2148 (2007).
10. T. M. Cover and P. E. Hart, IEEE Trans. Inf. Theory **13**, 21–27 (1967).
11. F. Pedregosa, G. Varoquaux, A. Gramfort, V. Michel, B. Thirion, O. Grisel, M. Blondel, P. Prettenhofer, R. Weiss, V. Dubourg, J. Vanderplas, A. Passos, D. Cournapeau, M. Brucher, M. Perrot, and E. Duchesnay, J. Mach. Learn. Res. **12**, 2825–2830 (2011).
12. N. Japkowicz and M. Shah, *Evaluating learning algorithms: a classification perspective* (Cambridge University Press, 2011).
13. O. Matoba, T. Nomura, E. Pérez-Cabré, M. S. Millán, and B. Javidi, Proc. IEEE **97**, 1128—1148 (2009).
14. A. Alfalou and C. Brosseau, Adv. Opt. Photonics **1**, 589–636 (2009).
15. P. Clemente, V. Durán, E. Tajahuerce and J. Lancis, Opt. Lett. **35**, 2391-2393 (2010).
16. Y. Rivenson, A. Stern and B. Javidi, Opt. Express **18**, 15094-15103 (2010).
17. W. Chen, B. Javidi, X. Chen, Adv. Opt. Photonics **6**, 120-155 (2014).

REFERENCES

1. J. M. Meruga, W. M. Cross, P. S. May, Q. Luu, G. A. Crawford, and J. J. Kellar, “Security printing of covert quick response codes using upconverting nanoparticle inks,” Nanotechnology **23**, 395201 (2012).
2. A. Markman, B. Javidi, and M. Tehranipoor, “Photon-counting security tagging and verification using optically encoded qr codes,” IEEE Photon. J. **6**, 1–9 (2014).
3. A. Carnicer, A. Hassanfiroozi, P. Latorre-Carmona, Y.-P. Huang, and B. Javidi, “Security authentication using phase-encoded nanoparticle structures and polarized light,” Opt. Lett. **40**, 135–138 (2015).
4. V.-M. Freire, C. Corbella, E. Bertran, S. Portal-Marco, M. Rubio-Roy, and J.-L. Andújar, “Anisotropic surface properties of micro/nanostructured ac: H: F thin films with self-assembly applications,” J. Appl. Phys. **111**, 124323 (2012).
5. C. Corbella, B. Echebarria, L. Ramírez-Piscina, E. Pascual, J. Andújar, and E. Bertran, “Spontaneous formation of nanometric multilayers of metal-carbon films by up-hill diffusion during growth,” Appl. Phys. Lett. **87**, 213117 (2005).
6. O. Arteaga, M. Baldrís, J. Antó, A. Canillas, E. Pascual, and E. Bertran, “Mueller matrix microscope with a dual continuous rotating compensator setup and digital demodulation,” Appl. Opt. **53**, 2236–2245 (2014).
7. O. Arteaga, “Useful mueller matrix symmetries for ellipsometry,” Thin Solid Films **571**, 584–588 (2014).
8. J. L. Horner and P. D. Gianino, “Phase-only matched filtering,” Appl. Opt. **23**, 812–816 (1984).
9. T. Nomura and B. Javidi, “Object recognition by use of polarimetric phase-shifting digital holography,” Opt. Lett. **32**, 2146–2148 (2007).
10. T. M. Cover and P. E. Hart, “Nearest neighbor pattern classification,” IEEE Trans. Inf. Theory **13**, 21–27 (1967).
11. F. Pedregosa, G. Varoquaux, A. Gramfort, V. Michel, B. Thirion, O. Grisel, M. Blondel, P. Prettenhofer, R. Weiss, V. Dubourg, J. Vanderplas, A. Passos, D. Cournapeau, M. Brucher, M. Perrot, and E. Duchesnay, “Scikit-learn: Machine learning in Python,” J. Mach. Learn. Res. **12**, 2825–2830 (2011).
12. N. Japkowicz and M. Shah, *Evaluating learning algorithms: a classification perspective* (Cambridge University Press, 2011).
13. O. Matoba, T. Nomura, E. Pérez-Cabré, M. S. Millán, and B. Javidi, “Optical techniques for information security,” Proc. IEEE **97**, 1128—1148 (2009).
14. A. Alfalou and C. Brosseau, "Optical image compression and encryption methods," Adv. Opt. Photonics **1**, 589–636 (2009).
15. P. Clemente, V. Durán, E. Tajahuerce and J. Lancis, "Optical encryption based on computational ghost imaging," Opt. Lett. **35**, 2391–2393 (2010).
16. Y. Rivenson, A. Stern and B. Javidi, "Single exposure super-resolution compressive imaging by double phase encoding," Opt. Express **18**, 15094–15103. 2010.
17. W. Chen, B. Javidi, and X. Chen, "Advances in optical security systems," Adv. Opt. Photonics **6**, 120-155 (2014).